Electrostatic Force Spectroscopy and Imaging of Bi Wires: Spatially Resolved Quantum Confinement

D. Gekhtman,[1] Z. B. Zhang,[1] D. Adderton,[2] M. S. Dresselhaus,[1,3] and G. Dresselhaus[4]
[1]*Department of Physics, Massachusetts Institute of Technology, Cambridge, Massachusetts 02139*
[2]*Digital Instruments, Santa Barbara, California 93117*
[3]*Department of Electrical Engineering and Computer Science, Massachusetts Institute of Technology, Cambridge, Massachusetts 02139*
[4]*Francis Bitter Magnet Lab, Massachusetts Institute of Technology, Cambridge, Massachusetts 02139*
(Received 20 January 1999)

We demonstrate that scanning probe electrostatic force microscopy applied to a nanoscale electronic structure can be used for studying the spatially resolved carrier quantized states as determined by the screening properties of local surface regions of the structure. The results presented for the cross-sectional surface of Bi quantum wires elucidate the microscopic nature of quasi-one-dimensional confined states excited by an applied bias voltage, where the single-particle-in-a-box energy quantization competes with the wire boundary enhanced intercarrier Coulomb repulsion. [S0031-9007(99)09105-X]

PACS numbers: 73.20.At, 71.10.Ca, 73.20.Dx, 73.61.Tm

The invention of the atomic force microscope [1] (AFM) has opened a new era of scanning force experiments. The second generation electrostatic force microscopy [2] (EFM) allows us to study spatially resolved ($\sim$1 nm) electronic properties of surfaces containing both conducting and insulating regions, and, therefore, this technique can be applied to nanoscale quantum heterostructures. EFM measures the axial gradient of the electrostatic force acting on a small biased probe as a result of the long-range Coulomb interaction with the near-surface charges of the structure. So far, EFM has been successfully applied to detecting surface trapped charges [3], to profiling the dopant concentration in microdevices [4], and to measuring work functions [5] of various materials.

Here we show how EFM can be employed to study the screening properties of a quasi-one-dimensional (1D) electron (or hole) gas excited near the cross-sectional surface of Bi quantum wires by applying a bias voltage (V_b) with respect to the nearby probe. The study reveals that EFM bias voltage spectroscopy and imaging, observed at probe-wire distances (h) nearly comparable to the Thomas-Fermi screening length (λ) of the wire carriers, provide direct information on the 1D-quantized carriers states as a function of energy and spatial position. At these small distances ($h \sim 10$ nm), the electrostatic attraction between the Bi wire and the capacitively coupled probe is reduced as a result of the penetration of an electric field, associated with the charged probe, into the wire subsurface region. Assuming the simplest case of a plane capacitor [6] geometry formed by the probe tip and the local surface region of the wire, the attractive electrostatic force gradient (F') acting between them is, then, to first order in (λ/h) given by

$$F' = \frac{S(V_b - V_0)^2}{4\pi(h + \lambda)^3}, \qquad \lambda \equiv (4\pi e^2 \partial n/\partial\mu)^{-1/2}. \quad (1)$$

In Eqs. (1), S denotes the probe tip area, eV_0 is the electron work function of the Bi wire relative to that of the probe, and λ, within the linear screening theory, is inversely related to the carrier thermodynamic density of states (TDOS) $\partial n/\partial\mu$, where μ is the wire electrochemical potential controlled by the bias voltage V_b. Thus, we study the TDOS of a single wire for various wire radii $30 \leq R < 70$ nm by measuring F' as a function of the probe position in both the diametrical (x) and axial (z) directions, as well as by the bias voltage spectroscopy of F' obtained at a given point (x, z) above the wire cross-sectional surface (see Fig. 1).

The single-crystal Bi wires used in this study were grown [7] as arrays of parallel wires embedded in insulating Al_2O_3 templates, as shown in Fig. 1. Since the dielectric constant of the Al_2O_3 template is low [8],

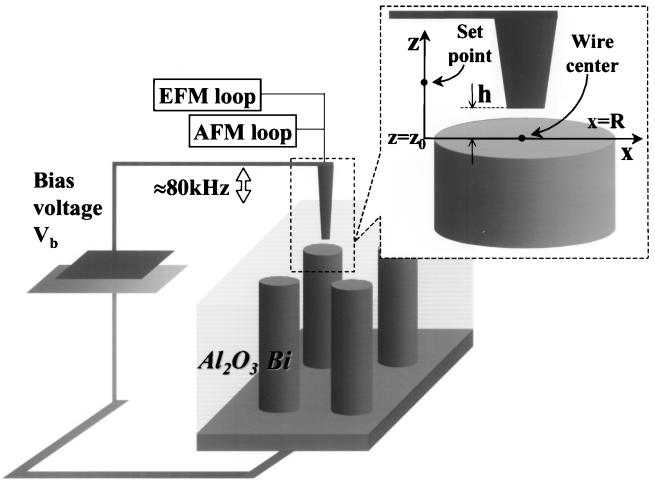

FIG. 1. Experimental details and geometry for the scanning force study of Bi quantum wires. The probe location above the cross-sectional surface of a single wire of radius R is measured with respect to the wire center in the diametrical direction x and with respect to the fixed set point in the axial direction z. (z_0 denotes the axial coordinate of the wire surface and $h \equiv z - z_0$ is the probe-wire distance.)

$\cong 1.3$, its surface dipole charges contribute negligibly to the measured F' and are, thus, disregarded in the following analysis. The measurements [9] are made by a two-pass procedure [10] using, consecutively, the tapping AFM and lift EFM modes, and operating near the resonant frequency ($\cong 80$ kHz) of the Au-coated etched silicon probe. In order to control the probe-wire distance h, which is, in general, not known precisely, we vary the lift-height z values in the range $-9 \leq z \leq 30$ nm with respect to a fixed set point (so that $h \equiv z - z_0$, Fig. 1), which is maintained constant throughout the measurement.

We calculate the 1D-quantized subband levels of the conduction and valence L-point energy bands for the $[10\bar{1}1]$ Bi wire growth direction, using the two-band Lax model [11] and the simplest particle-in-a-box confinement scheme. These energy bands possess the steepest (nearly linear) k dispersion in the wire cross-sectional surface plane, and, therefore, they contribute dominantly to the 1D singularities of the density of states. The 1D-subband edge energy levels, calculated for $R = 30$ nm, and the k dispersion of the bulk Bi bands are plotted in Fig. 2(a).

Figure 2(b) presents the V_b-spectroscopy of the measured F'. For bulk Bi, we observe small deviations of the measured V_b dependence from the parabolic fitting function [dashed curves in Fig. 2(b)], which is expected from classical electrostatics. These deviations, however, increase for the Bi wires with decreasing R, while clear oscillations develop. The observed oscillations are identified, by the normalized F'-spectra analysis, with the strong variations of the TDOS in the Bi wires, yielding a high TDOS (a low λ) as the wire electrochemical potential μ is raised by the external V_b to pass through the 1D-subband edges [see Eqs. (1)]. Then, in accordance with the calculated quantized levels shown in Fig. 2(a), the deepest minimum observed in each normalized F'-spectrum [see Fig. 2(b)] corresponds to the L-point quasigap, and this minimum becomes deeper as R decreases. The peaks observed below and above this quasigap minimum are attributed to the 1D-subband edges of the L-point conduction band (lower V_b) and valence band (higher V_b), respectively. A lack of symmetry between the observed conduction and valence band peaks can result from the effect of remote L-point bands as well as of the highest T-point valence band. The T-point band is expected to contribute mostly to the positive (hole) charge appearing near the wire surface, while applying a more positive bias voltage with respect to the minima of the fitting parabolas [shown by vertical arrows and denoted by V_0 in Fig. 2(b)]. These minima, to a good approximation, represent the relative position of the Bi electron work function eV_0 with respect to that of the probe. As can be seen from Fig. 2(b), with decreasing R, (i) the relative bias voltage position of V_0 with respect to $V_{L\,\mathrm{gap}}$ shifts towards the peak corresponding to the conduction subband; (ii) the value of V_0 moves towards a more positive bias voltage. Assuming

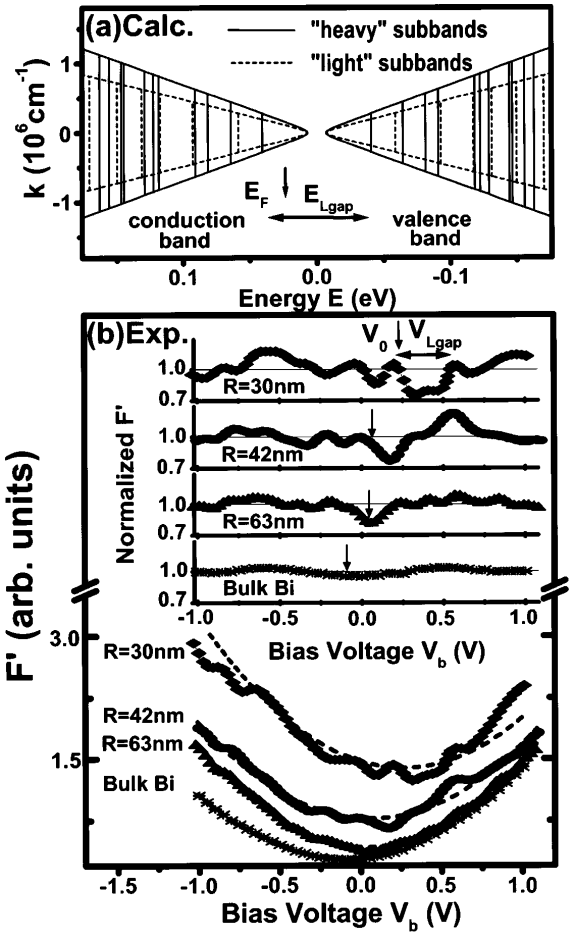

FIG. 2. (a) Bi L-point in-plane k dispersion and 1D-quantized energy levels (vertical bars correspond to $R = 30$ nm for "heavy" and "light" subband edges) of a $[10\bar{1}1]$-oriented wire calculated by particle-in-a-box quantization of the conduction and valence energy bands. The resulting quasigap $E_{L\,\mathrm{gap}}$ between the lowest conduction and highest valence subband levels is shown by the horizontal arrow. The vertical arrow indicates the position of the Fermi level E_F calculated relative to the quasigap midpoint, which is arbitrarily chosen to be at zero energy. (b) V_b-spectroscopy of the electrostatic force gradient (F') measured at $z = -3$ nm for bulk Bi as well as for Bi wires of various radii R near the wire boundary ($x \cong R$). The dashed curves are fitting parabolic functions. The curves plotted for $R = 30$ nm and for $R = 42$ nm are upshifted for clarity by 0.7 and 0.2, respectively. Also shown are the measured F' curves divided by the corresponding fitting parabolas (normalized F'). The vertical arrow indicates the minimum of the fitting parabola (V_0) and the horizontal arrow ($V_{L\,\mathrm{gap}}$) corresponds to the L-point quasigap (see text).

no dependence of the surface potential barrier on R, observation (i) would be consistent with the calculated shift of the Fermi level (E_F) deeper into the conduction band [Fig. 2(a)]. This shift is a result of phonon-assisted excitations from the nearest T-point band, being in thermal equilibrium with the L-point bands. However, our calculations [Fig. 2(a)] do not take into account surface effects and, therefore, cannot be used to explain rigorously the

apparent increase of the Bi wire work function with decreasing R [observation (ii)].

Two main factors are responsible for scaling up the calculated single-particle energy (E) by experimentally controlling V_b: (1) The electrostatic potential energy shift of the quantized energy spectrum, which to first order gives $\Delta E \cong -(\lambda/h)eV_b$; (2) the self-consistent nature of the carrier quantum confinement that results in an effectively smaller wire area occupied by bound states (see below), and, therefore, a larger energy separation between the 1D levels is observed. For example, the quasigap (peak-to-peak) values, extracted from Fig. 2(b) in units of the bias voltage, are $eV_{L\,\mathrm{gap}} \cong 370$, 305, and 220 meV for $R = 30$, 42, and 63 nm, respectively. On the other hand, the corresponding calculated energy values are $E_{L\,\mathrm{gap}} = 82$, 59, and 39 meV. We note that, although larger in absolute value, the measured quasigap has a nearly linear dependence on R^{-1} (within 12%), in accordance with the calculation.

However, as we show below, the simplest single-particle quantum confinement scheme is not sufficient to describe even qualitatively the real space distribution of F', since the Coulomb interactions between the V_b-excited carriers strongly perturb the intrinsic quantum states. As presented in Fig. 3(a), the F' dependence on the probe diametrical position x shows an enhanced electrostatic attraction at the regions near the wire boundary circumference ($x \cong R$). This is opposite to the expected single-particle density of states distribution, which has a maximum at the wire center ($x = 0$) as a result of the quantum interference between the carrier waves reflected by the wire boundary. Figure 3(a) also shows that the near-boundary enhancement of the measured F' increases with decreasing z (or h), and this increase is more pronounced for the smaller wire radius $R = 30$ nm.

The underlying role of the intercarrier Coulomb repulsion for the explanation of the observed x dependence of F' can be understood in terms of a classical model considering the electrostatic field associated with the charged

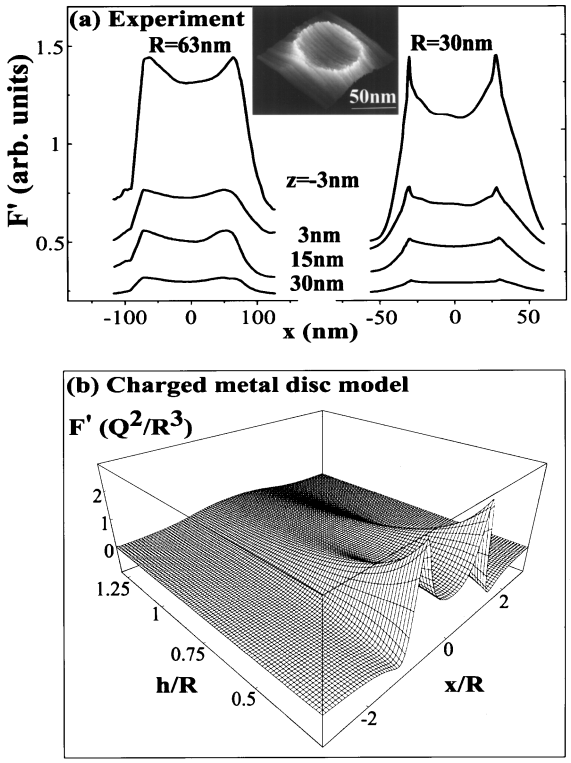

FIG. 3. Electrostatic force gradient (F'): (a) observed at $V_b = 0.98$ V for Bi wires of $R = 63$ nm (left column) and $R = 30$ nm (right column) by scanning the probe along the x axis at various z values; (b) calculated by Eq. (2), where $h \equiv z - z_0$ is the probe-wire distance. The inset of (a) shows an F'-image acquired at $z = 10$ nm for the $R = 30$ nm wire.

wire surface, approximated by a perfect metal disk of radius R, and felt by a pointlike oppositely charged probe at a distance h from the wire surface. Within this model, F' is proportional to the second derivative with respect to h of the electrostatic potential, which is, in turn, given by solving Laplace's equation in the free half-space with the equipotential disk boundary condition. The solution is found analytically [12] to be

$$F'(x,h) = \frac{Q^2}{R}\frac{\partial^2}{\partial h^2}\left[\arctan\left\{\left(\frac{x^2 + h^2 - R^2 + \sqrt{(x^2 + h^2 - R^2)^2 + 4h^2R^2}}{2R^2}\right)^{-1/2}\right\}\right], \tag{2}$$

where Q is the total induced charge [see Fig. 3(b)]. Thus, the increased attractive F', observed at $x \cong \pm R$, over that of $x = 0$ is reproduced by the model calculation [Eq. (2)], which gives $F'(R,h) - F'(0,h) \cong Q^2/(4R^{3/2}h^{3/2})$ for a small h/R ratio. This enhancement of F' near the boundary is essentially a result of the divergence of the surface charge density at $x = \pm R$ given by $\sigma(x) = Q/\{2\pi R^2(1 - x^2/R^2)^{1/2}\}$. The microscopic mechanism for such a classical inhomogeneous charge density distribution is the increased intercarrier Coulomb repulsion introduced by the confined conductor geometry.

Within the framework of classical theory, the contribution of the electrostatic attraction between the wire and the probe to $\sigma(x)$ (which is *not* taken into account in the above model) would be dominant at small h. However, for the case of the Bi wire, this contribution is weak since h is comparable to λ, so that the carrier density distribution induced near the wire surface does not manage to screen the electrostatic field of the scanning probe. Therefore, assuming a perfectly conducting probe with a negligible screening length, we can interpret the variations of F' with x, observed at small z (or h), in terms of a local effective screening length of the wire, which takes into account the intercarrier interactions self-consistently. The estimated λ for bulk Bi is $\cong 4$ nm, which, according to the extrapolated z dependence of $(F')^{-1/3}$ shown

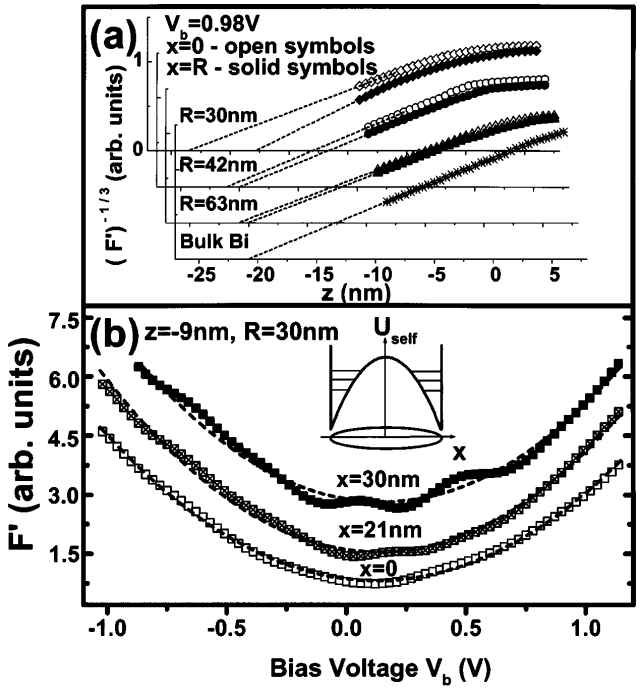

FIG. 4. (a) The z dependence of the electrostatic force gradient (F') measured under $V_b = 0.98$ V for bulk Bi as well as for the Bi wires of various R near the boundary ($x = R$) and at the center ($x = 0$). The dashed lines extrapolate the plotted values of $(F')^{-1/3}$ to small z values [see Eqs. (1)]. (b) V_b-spectroscopy of F' measured for the $R = 30$ nm wire at $z = -9$ nm and at various points along the x axis. The dashed curves are the parabolic fitting functions. The sketch shows schematically a self-consistent potential profile $U_{\rm self}(x)$ and the resulting quantized energy levels induced by the electrostatic charging of the wire.

in Fig. 4(a), gives [13] $z_0 \cong -17$ nm. Then, we find that λ is systematically lower (i.e., the TDOS is higher) near the wire boundaries than at the center, and this difference increases with decreasing R [Fig. 4(a)].

In Fig. 4(b), we show the V_b-spectroscopy of F' measured for $R = 30$ nm at a small value of $z = -9$ nm (corresponding to $h = z - z_0 \cong 8$ nm) and for various positions x on the wire surface. At this z value, the observed oscillations are stronger and more widely spaced in V_b (by more than 15%) than those observed at $z = -3$ nm [see Fig. 2(b)]. Also, the oscillations weaken dramatically as the probe moves in the x direction only by 9 nm ($\cong R/3$) towards the center of the wire surface. This proves that the induced carriers are squeezed quantum mechanically towards the wire boundaries by a self-consistent electrostatic charging potential ($U_{\rm self}$) for distances substantially smaller than R [see the sketch of $U_{\rm self}(x)$ and the quantized levels in Fig. 4(b)]. Obviously, $U_{\rm self}$ should depend on both V_b and z, since $U_{\rm self}$ is sensitive to the amount of induced charge that produces a classical-like charge density distribution over the wire surface.

In general, for materials with a quadratic $E(k)$, the self-consistent charging potential energy per particle, $\sim eQ/R$, becomes smaller than the quantization energy, $\sim \hbar^2/m^*R^2$, at a sufficiently small R. However, for the case of the Bi L-point energy bands with a nearly linear $E(k)$, the above charging energy does not become smaller than the quantization energy, since both are scaled by R^{-1} (in the range of $10 < R < 100$ nm). Assuming $Q \cong 10e$ (since the probe tip area is rather small), the charging energy is evaluated for $R = 30$ nm to be $\cong 480$ meV, which is substantially larger than the calculated energy separation between the quantized levels [Fig. 2(a)]. This explains why the charging effects are so appreciable for the observed quantum-confined 1D states in the Bi wires investigated in this work.

Support from Navy Contract No. N00167-98-K-0024, MURI/UCLA Subcontract No. 0205-5-7A114-01, and NSF-DMR-98-04734 are gratefully acknowledged. We also thank Supriyo Datta, Gang Chen, and Ray Ashoori for valuable discussions and Libby Shaw for technical help.

[1] G. Binnig, C. Quate, and Ch. Gerber, Phys. Rev. Lett. **56**, 930 (1986).
[2] Y. Martin *et al.*, Appl. Phys. Lett. **52**, 1103 (1988); J. E. Stern *et al.*, Appl. Phys. Lett. **53**, 2717 (1988).
[3] B. D. Terris *et al.*, Phys. Rev. Lett. **63**, 2669 (1989).
[4] A. K. Henning and T. Hochwitz, Mater. Sci. Eng. B **42**, 88 (1996).
[5] R. M. Nyffenegger, R. Penner, and R. Schierle, Appl. Phys. Lett. **71**, 1878 (1997).
[6] M. Büttiker, J. Phys. Condens. Matter **5**, 9361 (1993).
[7] Z. B. Zhang, J. Y. Ying, and M. S. Dresselhaus, J. Mater. Res. **13**, 1745 (1998).
[8] For example, *Handbook of Optical Constants of Solids*, edited by E. D. Palik (Academic Press, San Diego, 1991).
[9] For a review of scanning force principles, see O. Marti and J. Colchero, in *Forces in Scanning Probe Methods*, edited by J. J. Güntherodt, D. Anselmetti, and E. Meyer, NATO ASI Ser. E, Vol. 286 (Kluwer, Dordrecht, 1995).
[10] *Lift-Mode Operation Manual* (Digital Instrument Inc., Santa Barbara, CA, 1996).
[11] B. Lax and J. G. Mavroides, in *Advances in Solid State Physics*, edited by F. Seitz and D. Turnbull (Academic Press, New York, 1960), Vol. 11.
[12] J. C. Maxwell, *Treatise on Electricity and Magnetism* (Clarendon, Oxford, 1904).
[13] In the framework of classical electrostatics, taking into account a finite tip curvature would result in $F'(h)$ that is weaker than that given by Eqs. (1). Therefore, using the plane capacitor model for extrapolation of the measured $(F')^{-13}(z)$, as shown in Fig. 4(a), introduces a systematic overestimation of h.